Helsinki University of Technology
CFD-group/ Laboratory of Applied Thermodynamics
P.O.Box 4400
FIN-02015 HUT, FINLAND
Tel: +358 9 451 3949 Fax: +358 9 451 3418

MEMO No CFD/TERMO-21-97 DATE: November 3, 1997

TITLE

DESCRIPTION OF THE NUMERICAL METHODOLOGY FOR THE ERCOFTAC TEST CASE F3

AUTHOR(S)
Patrik Rautaheimo and Juha Ojala

ABSTRACT

The purpose of this work is to compare different low-Reynolds-number turbulence models and their suitability for the highly three dimensional return channel with a deswirl cascade. A comparison is made between Chien's $k-\epsilon$ model, Chien's model with a rotational correction, Gatski et al. ARSM and the full Reynolds stress model by Speziale et al.. Experiments are provided by Concepts ETI.

MAIN RESULT

Results for the test case F3 in the ERCOFTAC Workshop on Turbomachinery Flow Predictions VI

PAGES
16

KEY WORDS
Rotating machinery, turbulence models, $k-\epsilon$, RSM

APPROVED BY

Timo Siikonen November 3, 1997

1 General Description

A finite-volume CFD program FINFLO for complex three-dimensional geometries was used in the calculations. The program utilizes Cartesian velocity components in a cell-centred approach. The discretized equations are integrated in time by applying an implicit method. A multigrid V-cycle is applied for the acceleration of convergence. The main features of the numerical methods are described in [1].

2 Methods

2.1 Convection Scheme

In the evaluation of the inviscid fluxes, upwinding is used. For a spatial discretization a MUSCL-type scheme to approximate advective volume-face fluxes is applied. The scheme is based on a second-order upwinding in i-direction (in the flow direction) and a third-order upwind-biased in j- and k-directions. Roe's flux splitting [2] is employed in the calculation of fluxes.

2.2 Turbulence Models

Four different low-Reynolds number turbulence models were tested:

- $k-\epsilon$ model of Chien [3] (CH)
- $k-\epsilon$ model of Chien with a rotational correction (CHR)
- explicit ARSM of Gatski et al. [4] (GS)
- RSM of Speziale et al. [5] (SSG)

The first one is a classical low-Reynolds-number $k-\epsilon$ model (CH), the second one is Chien's $k-\epsilon$ model with rotational correction (CHR), the third one is an explicit algebraic Reynolds stress model (GS), and the fourth one is a full Reynolds stress closure (SSG).

$k-\epsilon$ Models

In general, models based on the solution of k- and ϵ-equations can be written as

$$\widetilde{\bar{\rho} u_i'' u_j''} = F(S_{ij}, W_{ij}, k, \epsilon, \mu_T) \quad (1)$$

$$\mu_T = c_\mu \, f_\mu \, \rho \, \frac{k^2}{\tilde{\epsilon}} \quad (2)$$

$$\epsilon = \tilde{\epsilon} + D \quad (3)$$

Table. 1: Functions and constants.

Model	D	$\tilde{\epsilon}_w$-B.C.	c_μ	$c_{\epsilon 1}$	$c_{\epsilon 2}$	σ_k	σ_ϵ
CH	$2\nu\frac{k}{y_n^2}$	$\nu\frac{\partial\tilde{\epsilon}}{\partial y_n}=0$	0.09	1.44	1.92	1.0	1.3
GS	0.0	$\nu 2\mu\left(\frac{\partial\sqrt{k}}{\partial y_n}\right)^2$	0.088	1.39	1.83	1.0	1.3

Model	f_μ	f_1	f_2	E
CH	$1.0-e^{-0.00115y^+}$	1.0	$1.0-0.22e^{-Re_T^2/36}$	$-2\mu(\tilde{\epsilon}/y_n^2)e^{-0.5y^+}$
GS	1.0	1.0	$1.0-e^{-Re_y/12.5}$	0.0

$$\frac{\partial\rho\,k}{\partial t}+\frac{\partial\rho\,u_i\,k}{\partial x_i} = \frac{\partial}{\partial x_i}\left[(\mu+\mu_T/\sigma_k)\frac{\partial k}{\partial x_i}\right]+P-\rho\,\epsilon \tag{4}$$

$$\frac{\partial\rho\,\tilde{\epsilon}}{\partial t}+\frac{\partial\rho\,u_i\,\tilde{\epsilon}}{\partial x_i} = \frac{\partial}{\partial x_i}\left[(\mu+\mu_T/\sigma_\epsilon)\frac{\partial\tilde{\epsilon}}{\partial x_i}\right]+c_{\epsilon 1}\,f_1\,\frac{\tilde{\epsilon}}{k}P-c_{\epsilon 2}\,f_2\,\frac{\rho\tilde{\epsilon}^2}{k}+E \tag{5}$$

Table 1 summarizes functions and constants for different turbulence models applied in this study. The production of turbulent kinetic energy P is written without additional modeling

$$P=\bar{\rho}\widetilde{u_i''u_j''}\frac{\partial u_i}{\partial x_j} \tag{6}$$

where Reynolds stresses $\bar{\rho}\widetilde{u_i''u_j''}$ are modeled in the CH model by using the Boussinesq approximation

$$\bar{\rho}\widetilde{u_i''u_j''}=-2\mu_T S_{ij}+\frac{2}{3}\delta_{ij}\rho\,k \tag{7}$$

Above S_{ij} is the mean strain rate tensor

$$S_{ij}=\frac{1}{2}\left(\frac{\partial u_i}{\partial x_j}+\frac{\partial u_j}{\partial x_i}\right) \tag{8}$$

With the explicit ARSM model of Gatski and Speziale [4] (GS) the Reynolds stresses are given by

$$\begin{aligned}\bar{\rho}\widetilde{u_i''u_j''} &= \frac{2}{3}\rho\,k\,\delta_{ij}-\frac{6(1+\eta^2)\alpha_1}{3+\eta^2+6\xi^2\eta^2+6\xi^2}\rho\frac{k^2}{\epsilon}[\left(S_{ij}-\frac{1}{3}S_{kk}\delta_{ij}\right)\\ &\quad+\alpha_4\frac{k}{\epsilon}\left(S_{ik}W_{kj}+S_{jk}W_{ki}\right)-\alpha_5\frac{k}{\epsilon}\left(S_{ik}S_{kj}-\frac{1}{3}S_{kl}S_{kl}\delta_{ij}\right)]\end{aligned} \tag{9}$$

where

$$W_{ij}=\frac{1}{2}\left(\frac{\partial u_i}{\partial x_j}-\frac{\partial u_j}{\partial x_i}\right) \tag{10}$$

is the mean vorticity tensor. In Eq. (9) η and ξ are strain rate invariants defined by

$$\eta=\frac{1}{2}\frac{\alpha_3}{\alpha_1}(S_{ij}S_{ij})^{\frac{1}{2}}\frac{k}{\epsilon}\qquad \xi=\frac{1}{2}\frac{\alpha_2}{\alpha_1}(W_{ij}W_{ij})^{\frac{1}{2}}\frac{k}{\epsilon} \tag{11}$$

Above α_1, α_2, α_3, α_4 and α_5 are the constants that assume the values from [6]

$$\begin{array}{llll} \alpha_1 = (\frac{4}{3} - C_2)g/2 & \alpha_2 = (2 - C_3)^2 g^2/4 & \alpha_3 = (2 - C_4)^2 g^2/4 & \\ \alpha_4 = (2 - C_4)g/2 & \alpha_5 = (2 - C_3)g & g = 1./(C_1/2 + C_5 - 1) & (12) \end{array}$$

and the pressure-strain-correlation model of Speziale et al. [5] is used

$$\begin{array}{llll} C_1 = 6.8 & C_2 = 0.36 & C_3 = 1.25 & \\ C_4 = 0.4 & C_5 = 1.88 & & (13) \end{array}$$

Rotational Correction

Chien's $k-\epsilon$ model was tested also with rotation correction. In the correction used the dissipation equation was modified so that the function f_2 is replaced by

$$f_2 = (1 - C_c)\left(1.0 - 0.22e^{-Re_T^2/36}\right) \tag{14}$$

where the term C_c has been added to account for Coriolis effects [7]. That term equals to $-0.2\,Ri$. The Richardson number Ri is calculated from

$$Ri = -\omega\,(s - \omega) \tag{15}$$

where the ω and s are nondimensional vorticity and strain rate [8]. The factor -0.2 is an empirically chosen constant.

Reynolds Stress Model

The Reynolds-stress model (RSM) can be written in the following form

$$\frac{\partial \bar{\rho}\widetilde{u_i'' u_j''}}{\partial t} + \frac{\partial(\bar{\rho}\tilde{u}_k \widetilde{u_i'' u_j''})}{\partial x_k} = P_{ij} + \Phi_{ij} + D_{ij} - \epsilon_{ij} \tag{16}$$

where P_{ij}, Φ_{ij}, D_{ij} and $\epsilon_{ij}$are the production term, the pressure-strain term, the diffusion term and the dissipation term, respectively.

The production term is exact, whereas the turbulent diffusion, the pressure strain and the dissipation rate must be modeled. In this work the high-Reynolds number modeling is developed by Speziale, Sarkar and Gatski (hereafter referred as SSG) [5]. The low-Reynolds number modeling is based on Shima's work [9]. The connection of the low and high Reynolds number regions is done in a similar way as in [10]. In both cases the dissipation transport equation is based on Chien's $k-\epsilon$ model [3]. More details can be found from Rautaheimo et al. [11].

3 Results

3.1 Mesh

Only one deswirl channel is modeled. The grid is divided into three blocks, the first block is at the U-bend, the second one is an O-type grid over a deswirl

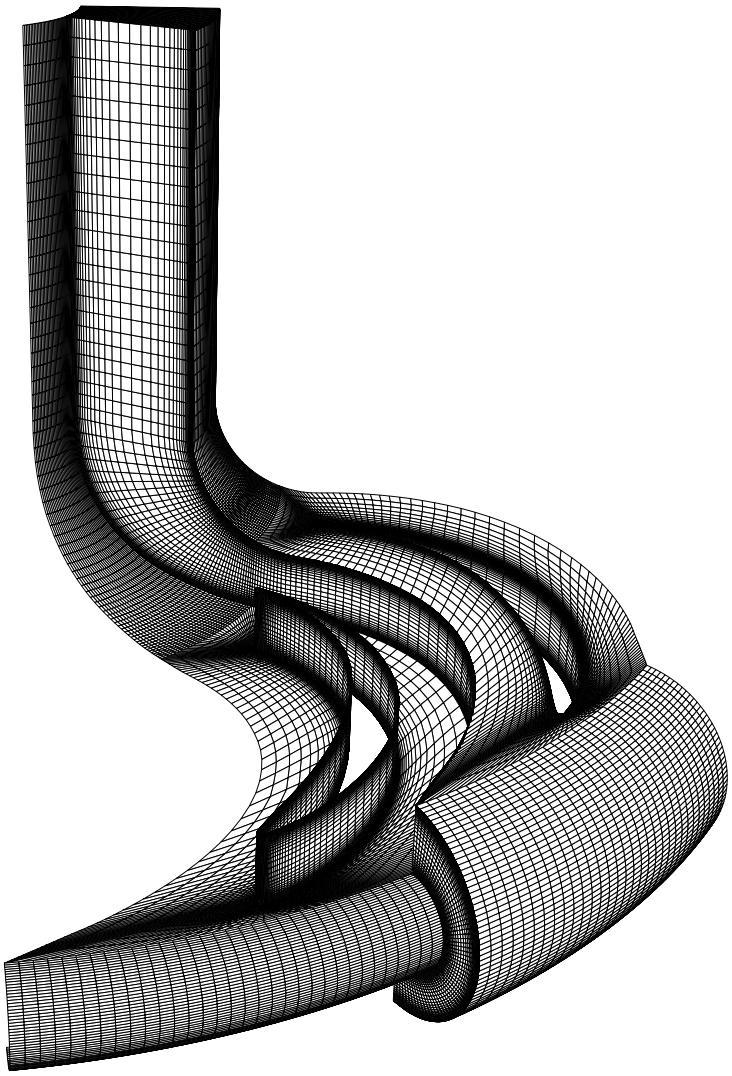

Fig. 1: Computational grid.

cascade, and the third one is after the cascade. The grid can be seen in Fig. 1 and the dimensions in Table 2. The height of the first row of cells is 6×10^{-6}m. As nondimensional distances this is on the average $y^+ \approx 1$ but on the leading edge y^+ has a maximum value of 6 in a very small area. Values of y^+ are shown in Fig. 2.

3.2 Boundary Conditions

The return channel has calculated only for AAB operation point in present work. Calculation begins at station 5. The velocities were interpolated from measurement points to the computational grid. Because measurement grid was quite a coarse the mass flow rate was not achieved with AAB operation point. Because of this the inlet velocities were multiplied by a factor of 1.0476. For turbulence quantities the 10% turbulence intensity was assumed and the

Table. 2: Dimensions of the grid.

Block	i	j	k	Σ
1	64	32	64	131 072
2	192	32	64	393 216
3	64	32	64	131 072
Total				655 360

Table. 3: Convergence of the test cases.

Model	CFL	Multigrid levels	Iteration cycles	L_2 level
Chien	2.0	4	1 200	$5 \cdot 10^{-8}$
Chien rot	2.0	3	1 500	$5 \cdot 10^{-7}$
GS	2.0	3	3 000	$2 \cdot 10^{-6}$
SSG	2.0	4	1 200	$2 \cdot 10^{-7}$

dissipation was assigned so that nondimensional turbulence viscosity (μ_T/μ) was 100 in order to get fully turbulent inflow. Using these boundary conditions a small jump in the calculated values takes place after the inlet. A more detailed study could be done with the inlet turbulence profiles, but present simple method seems to work well. For Reynolds stresses isotropic flow is considered and the shear stresses are assumed to be zero. At the outflow slot the static pressure is fixed and zero gradient is assumed for the rest of the variables. To avoid errors from the outlet, station 8 was eight grid cells before the outflow slot.

3.3 Convergence and Turn-Around Time

Convergence criterion was based on the L2 norms of the u-momentum residuals. Convergence parameters are shown in Table 3, where L_2 is the norm of the u-momentum residual. The CH and SSG models have satisfactory convergence behaviour. In the GS model the solution had small oscillation in front of the deswirl cascade, but the integrated values did not oscillate. The CHR result oscillates at both bends. In Fig. 3 the L_2 norm of u-momentum residuals are shown. From this figure it can be seen that the CH model has the best convergence rate. Also the CHR has good convergence at the beginning of the calculation, but after 400 iteration cycles the solution became oscillatory.

Computation was performed with the SGI Origin2000. The maximum memory required was 350 Mbytes for the two equation models and 570 Mbytes for RSM. The code was run in a parallel mode with two processors [12]. Com-

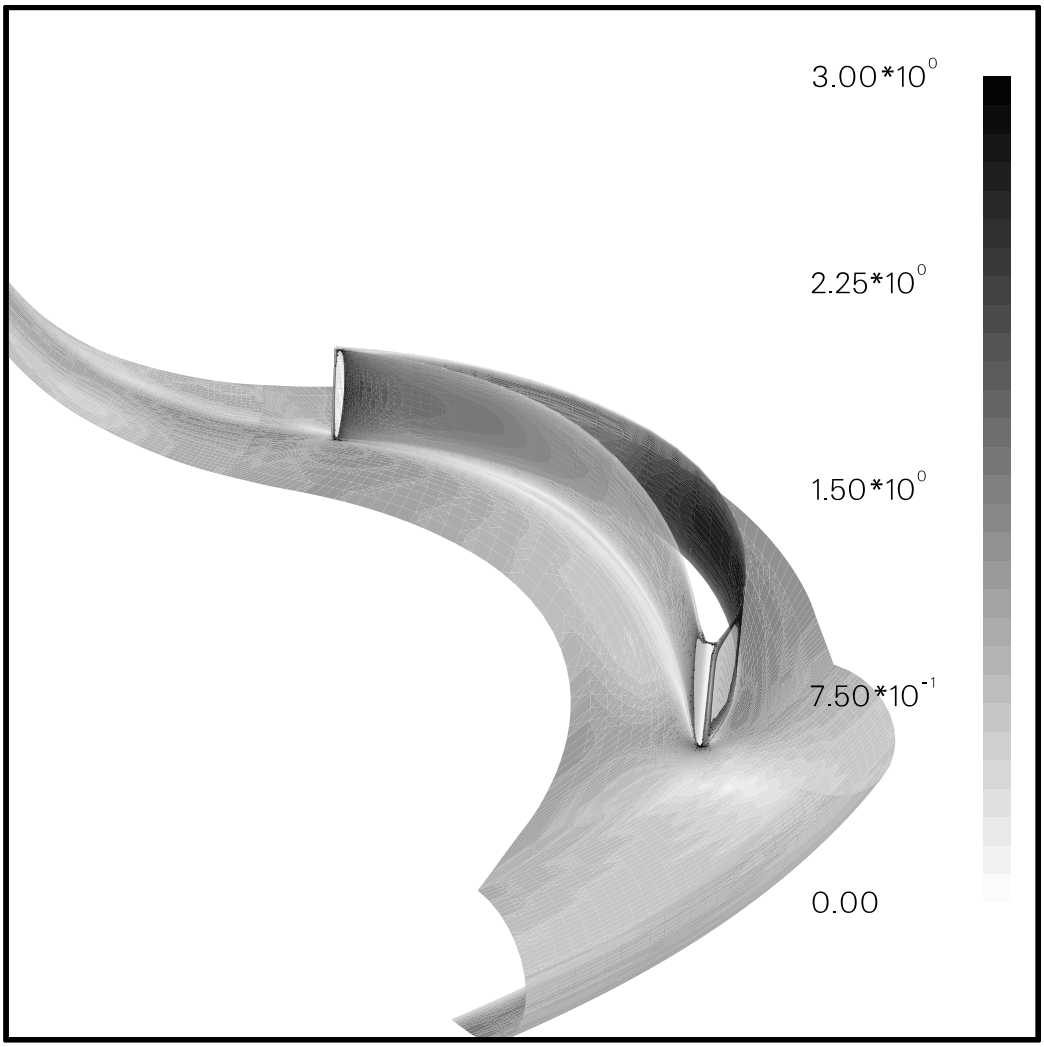

Fig. 2: Value of y^+ in the first grid point.

putational time was 45 seconds per cycle with the $k-\epsilon$ model, 46 seconds per cycle with ARSM and 90 seconds with the full RSM.

The grid was made in 10 hours and routines to interpolate the boundary conditions in a required format took about 6 hours. Computation of one test case took less than 24 hours. This could be reduced to 8 hours with a more efficient parallelization strategy and 5 parallel nodes.

3.4 Global Parameters

Global parameters are shown in Table 4, where $\dot{m}_{inlet}$, $\dot{m}_{outlet}$, $\Sigma\rho_i V_i k_i$ and $\Sigma\rho_i V_i \epsilon_i$ are values for 1/14 of the whole channel. Variables $\Sigma\rho_i V_i k_i$ and $\Sigma\rho_i V_i \epsilon_i$ are calculated over the whole computational domain, where V_i is a volume of a computational cell.

From the calculated mass flows $\dot{m}_{inlet}$ and $\dot{m}_{outlet}$ it is seen that computations are practically converged. Small differences come from numerics. The

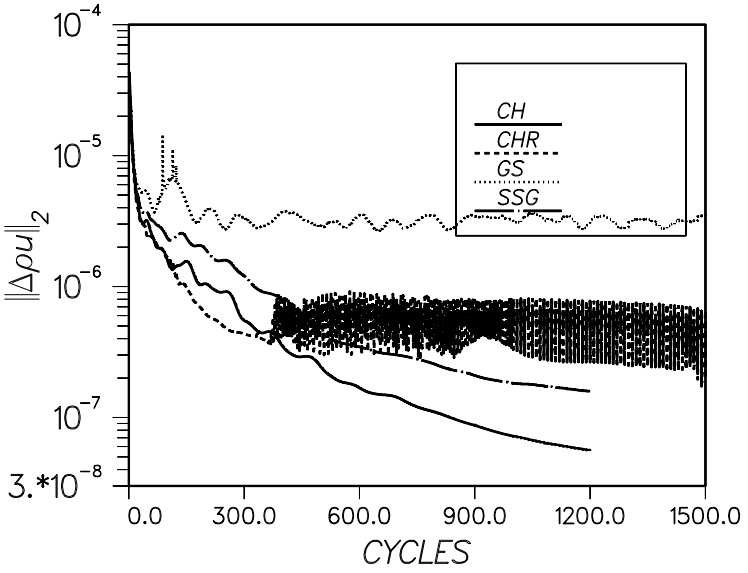

Fig. 3: L_2 norm of u-momentum residuals.

Table. 4: Global parameters.

	$\dot{m}_{inlet}$ (kg/s)	$\dot{m}_{outlet}$ (kg/s)	Δp_0 (N/m^2)	$\Sigma\rho_i V_i k_i$ 10^{-3} (J)	$\Sigma\rho_i V_i \epsilon_i$ (W)
Exp.	0.02204	0.02204	1977	-	-
CH	0.02204	0.02217	730	4.51	7.67
CHR	0.02204	0.02231	3000	25.8	15.5
GS	0.02203	0.02231	760	4.00	8.83
SSG	0.02204	0.02233	880	4.10	8.42

total pressure drop is quite small in comparison with the pressure level, and it seems that numerical errors may have some effect in the calculation of Δp_0. Experimental values are taken by averaging the total pressures at stations 5 and 8. Total pressures are averaged by using mass flow weighting. Variables $\Sigma\rho_i V_i k_i$ and $\Sigma\rho_i V_i \epsilon_i$ show the turbulence level predicted by different turbulence models. If the total pressure drop is compared with turbulence parameters the relation is clearly visible. The difference between the SSG and GS models may be because the low-Reynolds number version of SSG model generally overpredicts the skin friction. One reason for the higher total pressure drop of the experimental data can be explained if the walls are not hydrodynamically smooth. The CHR model overpredicts the total pressure drop as well as the turbulence level in comparison with the experimental data and other calculations.

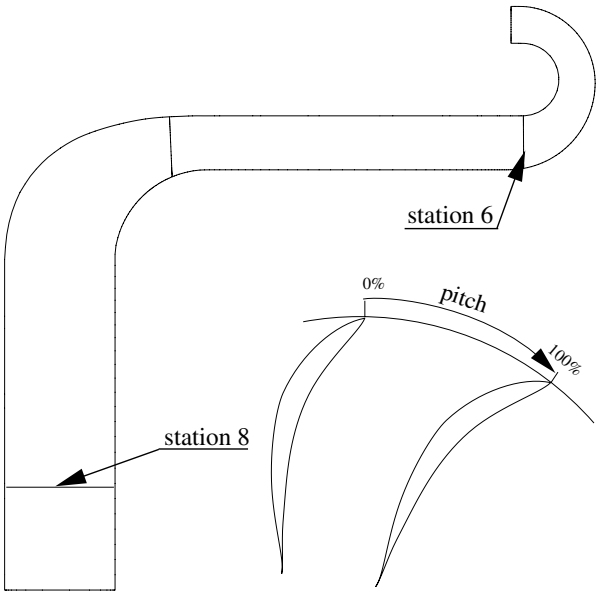

Fig. 4: Location of stations 6 and 8 and different pitch percents.

3.5 Calculated Profiles at Different Stations

Station 6

Measurement stations can be seen in Fig. 4. Profiles for the meridional and tangential velocities are shown at station 6 in Figs. 5 and 6. The SSG and GS models seem to predict the flow better than the simpler CH and CHR models. For example the tangential velocity at blade pitch 60% (Fig. 6) contains a peek close to the hub that is predicted by the SSG model. Also the GS model predicts the peek, but it is smaller. The CH and CHR models do not seem to predict this phenomena. All turbulence models have difficulties at the shroud at the pitch values 20%, 50%, 60% and 80%. They underpredict the meridional velocities and overpredict the tangential velocities. The size of the separation bubble is seen from the meridional velocities in Fig. 5. The SSG model predicts the strength and the size of the bubble well. The CH and CHR models do not have separation bubble at all at this station.

Pitch Averaged Values at Stations 6 and 8

Pitch averaged values are shown in Figs. 7 and 8. The computed results are averaged using five values at the same points, where the measurements (20, 40, 50, 60 and 80 percents of pitch) have been done. In this way the computed and measured averaged values were considered to be the same. Since no experimental data was available, the turbulence quantities are averaged over the whole domain. Meridional and tangential velocities are predicted well near the hub with the SSG model. Again the velocities next to the shroud are not well predicted by any of the turbulence models.

It can be seen that the CHR model predicts the highest turbulence level at

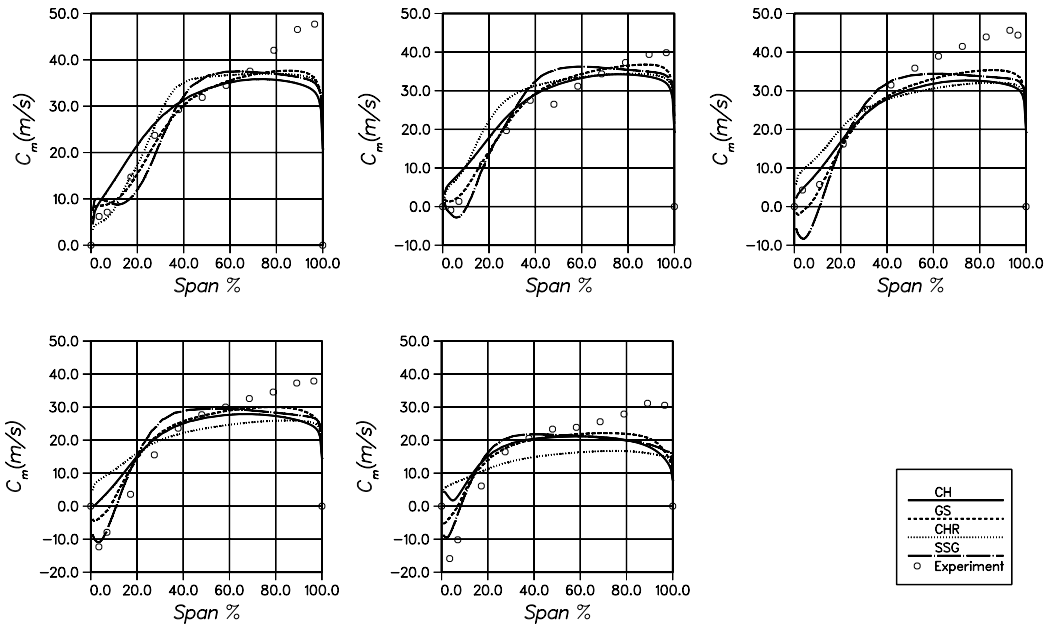

Fig. 5: Meridional velocity at the blade pitches of 20, 40, 50, 60 and 80 percents from the hub to the shroud (station 6).

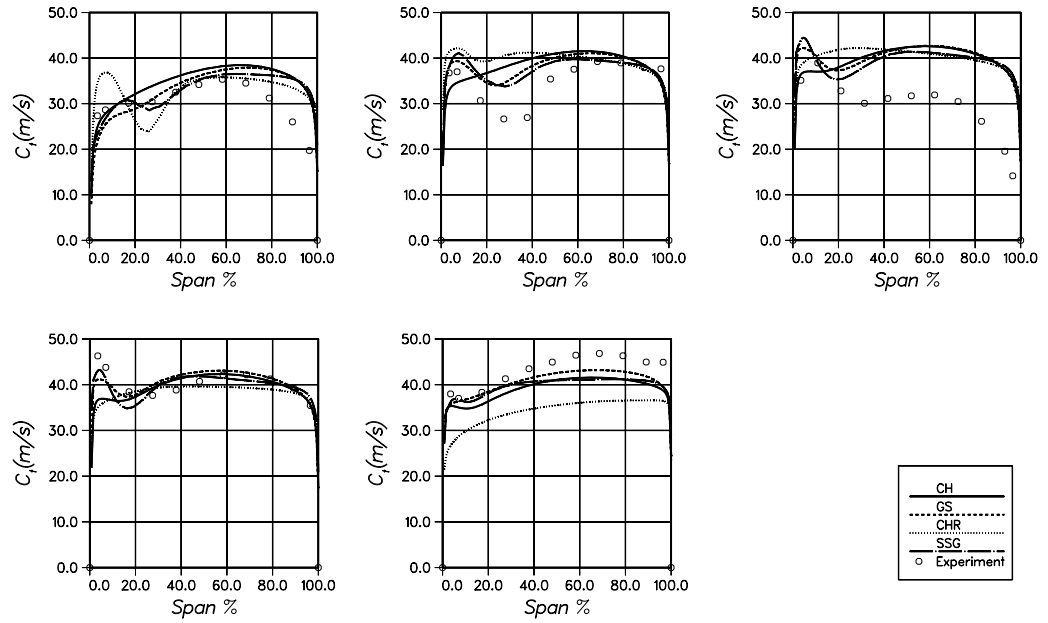

Fig. 6: Tangential velocity at the blade pitches of 20, 40, 50, 60 and 80 percents from the hub to the shroud (station 6).

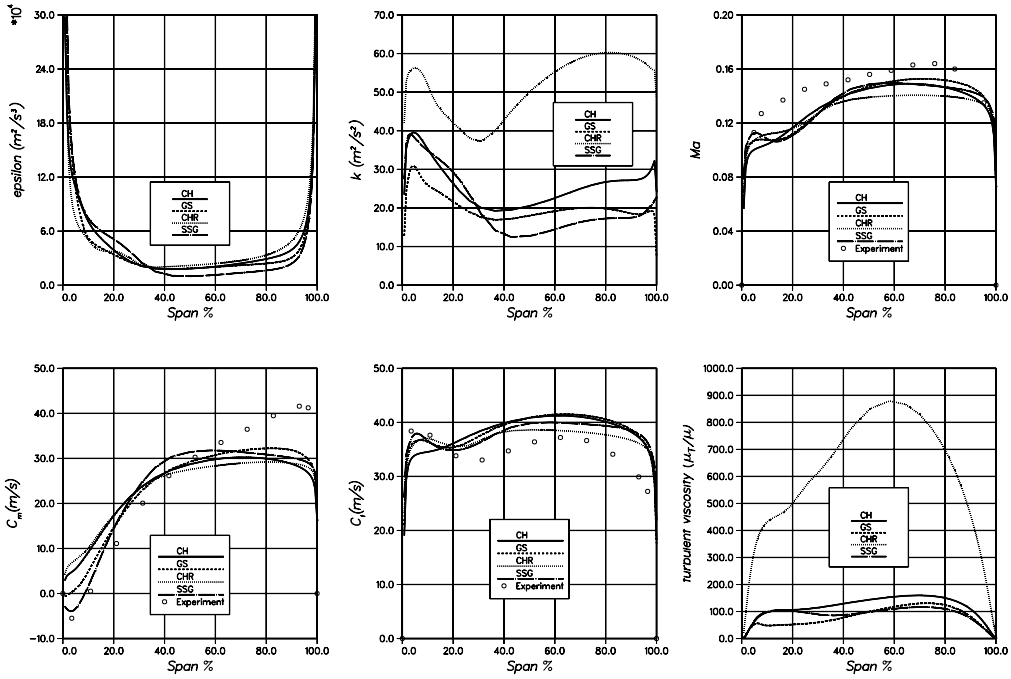

Fig. 7: Pitch averaged ϵ, k, Ma, meridional and tangential velocities and turbulent viscosity from the hub to the shroud at station 6.

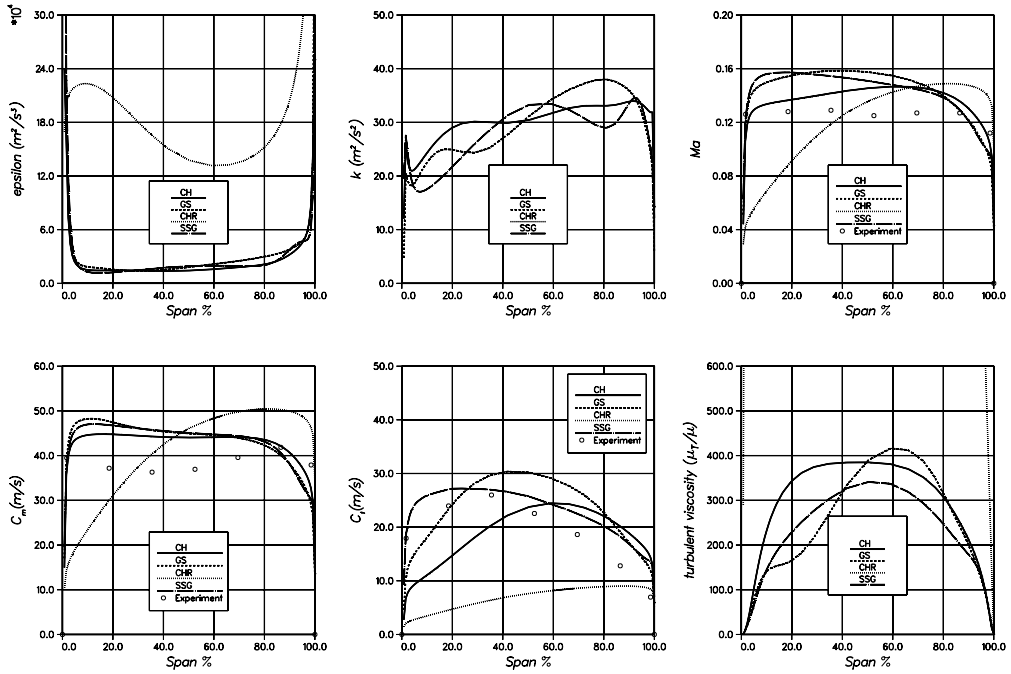

Fig. 8: Pitch averaged ϵ, k, Ma, meridional and tangential velocities and turbulent viscosity from the hub to the shroud at station 8.

both stations. At station 6 it predicts the flow field quite well, but at station 8 it is far from the experiments. It can be concluded that the rotative correction in a suggested form does not work properly in the present case.

3.6 Particle Traces at the Center of the Channel

Particle traces have been drawn at the center of the channel in Fig. 9. The CH model does not predict the separation after the U-bend. The CHR model predicts the separation but it seems to take place too early and it also reattaches too early. The GS and SSG models have separation bubbles just after the bend.

4 Discussion

The anisotropic models GS and SSG seem to behave better than the Boussinesq approximation based CH and CHR models. This is due to the curvature of the flow case which causes difficulties for isotropic models. Rotational correction is ad hoc in nature and it has been optimized by the present authors for Johnston rotating channel [13] and applied successfully for a pump. In this case it does not work, but a similar tuned correction could be built for this case also.

The GS model gives similar results to those of the SSG model but it has problems with stability. The SSG converges surprisingly well in this case. The overall computational work is equal to that of the GS model, because the GS model needs more iteration cycles. As expected the simple CH model has the best convergence rate.

No model predicts correctly the total pressure drop Δp_0. Although the SSG model gives a better total pressure drop than the GS model, this could be because of the present low-Reynolds number corrections generally overpredict the skin friction. More detailed comparison of flow variables along to the channel should be done.

Surface stream lines give some interesting small details about the simulated flow field (Figures are in the appendix). At the leading edge of the vane separation occurs on the pressure side with the CHR, GS and SSG models. The CH model does not predict this feature. In the CHR and GS models the shape of the separation bubble is quite similar. In the SSG model the separation bubble is very small and close to the leading edge. Also at the trailing edge (a small figure on the right hand side) the shape of the separation region is predicted differently by the turbulence models. The GS model predicts the largest separation region, the CHR and CH models predict quite the same sized separation bubbles but with the SSG model flow remain attached. When using the CHR model, the flow separates at the bend after the cascade. This and other results confirm that the CHR model does not work well in this case.

In complex geometries with streamline curvature, 3D effects and flow separations cannot be simulated by standard $k-\epsilon$ models. This is due to the iso-

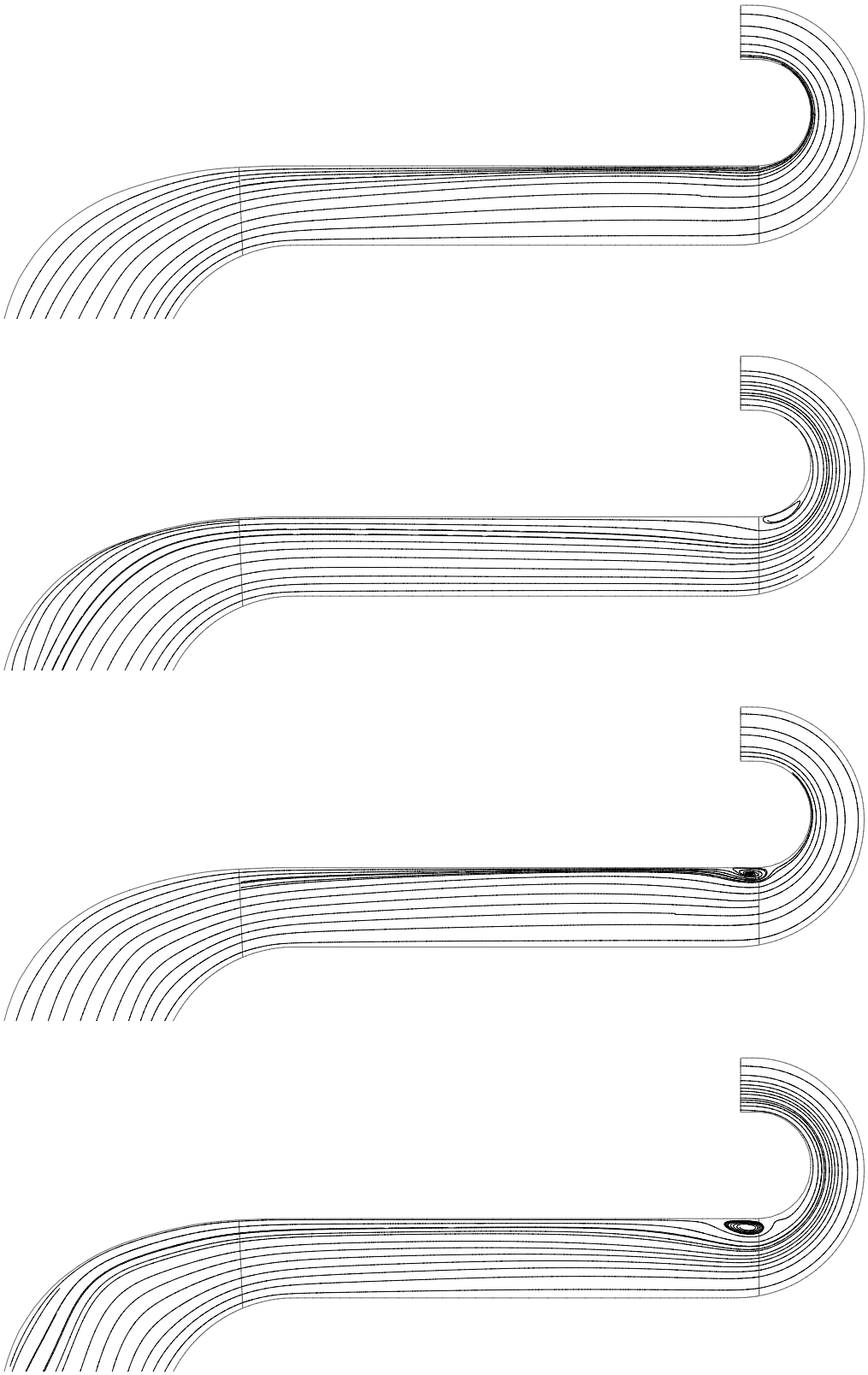

Fig. 9: Particle traces in the center of channel (CH, CHR, GS and SSG).

tropic Boussinesq-approximation and also the history effect of different Reynolds stresses. That is why in the present work anisotropic models behave better. The best results are achieved by the SSG model although there are certain features that are systematically ill-predicted by all turbulence models. Also the GS model gives satisfactory results for some details not captured by the basic CH model.

References

[1] Siikonen, T., "An Application of Roe's Flux-Difference Splitting for the $k-\epsilon$ Turbulence Model," *International Journal for Numerical Methods in Fluids*, Vol. 21, 1995, pp. 1017–1039.

[2] Roe, P., "Approximate Riemann Solvers, Parameter Vectors, and Difference Schemes," *Journal of Computational Physics*, Vol. 43, 1981, pp. 357–372.

[3] Chien, K.-Y., "Predictions of Channel and Boundary-Layer Flows with a Low-Reynolds-Number Turbulence Model," *AIAA Journal*, Vol. 20, Jan 1982, pp. 33–38.

[4] Gatski, T. and Speziale, C., "On explicit algebraic stress models for complex turbulent flows," *Journal of Fluid Mechanics*, Vol. 254, 1993, pp. 59–78.

[5] Speziale, C., Sarkar, S., and Gatski, T., "Modelling the pressure-strain correlation of turbulence: and invariant dynamical systems approach," *Journal of Fluid Mechanics*, Vol. 227, 1991, pp. 245–272.

[6] Abid, R., Rumsey, C., and Gatski, T., "Prediction of Nonequilibrium Turbulent Flows with Explicit Algebraic Stress Models," *AIAA*, Vol. 33, No. 11, 1995, pp. 2026–2031.

[7] J. H. G. Howard, S. V. P. and Bordynuik, R. M., "Flow Prediction in Rotating Ducts Using Coriolis-Modified Turbulence Models," *Journal of Fluids Engineering*, Vol. 102, December 1980.

[8] Khodak, A. and Hirsch, C., "Second Order Non-Linear k-ϵ Models with Explicit Effect of Curvature and Rotation," in *Proceedings of the Third ECCOMAS Congress*, (Paris), Sept. 1996.

[9] Shima, N., "A Reynolds-Stress Model for Near-Wall and Low-Reynolds-Number Regions," *Journal of Fluids Engineering*, Vol. 110, 1988, pp. 38–44.

[10] Chen, H.-C., "Assessment of a Reynolds Stress Closure Model for Appendage-Hull Junction Flows," *Journal of Fluids Engineering*, Vol. 117, Dec 1995, pp. 557–563.

[11] Rautaheimo, P. and Siikonen, T., "Implementation of the Reynolds-stress Turbulence Model," in *Proceedings of the Third ECCOMAS Congress*, (Paris), Sept. 1996.

[12] Rautaheimo, P., Salminen, E., and Siikonen, T., "Parallelization of a Multi-Block Navier–Stokes Solver," in *Proceedings of the ECCOMAS Congress*, (Paris), Sept. 1996.

[13] James P. Johnston, R. M. H. and Lezius, D. K., "Effects of spanwise rotation on the structure of two-dimensional fully-developed turbulent channel flow," *Journal of Fluid Mechanics*, Vol. 56, December 1972.